Supporting Information

Liu et al. 10.1073/pnas.1201105109

SI Materials and Methods

Mice, Tumor Harvesting, Single-Cell Preparation, and Enrichment of lin$^-$ Epithelial Cells. Mammary tumors (0.5–1.0-cm diameter) and glands were dissected from MMTV-Neu mice (1), fixed in 4% (wt/vol) paraformaldehyde and analyzed as described (2, 3). To generate single-cell suspension by the enzymatic method, a portion of the tumor was minced into small pieces with sterile razor blade, washed in PBS, digested in 100 U/mL collagenase/hyaluronidase (StemCell Technologies; no. 07912) for 1 h at 37 °C with occasional mixing, and washed once with 5× HBSS (Sigma; phenol red free; no. H4891) plus 2% (wt/vol) FBS and 1 mM EDTA (HFE). For the mechanical method, minced tumor tissue was resuspended in 10 mL of HFE and passed through an 18-gauge needle five times. Single-cell suspensions from enzymatic or mechanical preparations were centrifuged at 70 × *g*, supernatant discarded, and pellet resuspended in 10 mL of HFE, followed by passing through a 40 μm cell strainer (BD Falcon; no. 352340). Selective depletion of endothelial (anti-CD31; BD PharMingen) and hematopoietic cells (anti-CD45 and anti-TER119; StemCell Technologies) was accomplished with magnetic beads using a Mammary Stem Cell Enrichment kit from StemCell Technologies (no. 19757). We found that the inclusion of anti-CD140a antibodies to deplete fibroblasts was not necessary for Neu tumors (n = 4).

Flow Cytometric Analysis and Sorting. For flow cytometry, we used anti-CD49f conjugated with R-phycoerythrin (CD49f-PE, clone GoH3, 5 μL/million cells; BD Pharmingen; no. 555736), anti-CD24 conjugated with fluorescein isothiocyanate (CD24-FITC, clone M1/69, 0.25 μg/million cells; BD Pharmingen; no. 553261), anti-Sca1 conjugated with R-phycoerythrin (Sca1-PE, clone E13-161.7, 0.25 μg/million cells; BD Pharmingen; no. 553108), rabbit-anti-Jagged1 (Cell Signaling; clone 28H8, 1:250 dilution; no. 2620), biotin-anti-Notch1 (BioLegend; clone mN1A, 1:250 dilution; no. 629104), and mouse-anti-HER2 (CalBiochem; clone Ab-4, 1:250 dilution; no. OP16). For Jagged1, we used secondary biotin–anti-rabbit antibody (Vector; no. BA-1000), followed by APC-Streptavidin (BD Pharmingen; no. 554067); Notch1, APC-Streptavidin; and HER2, anti-mouse Ig conjugated with R-phycoerythrin (BD Pharmingen; no. 559940). Cells were suspended in HBSS plus 2% FBS and 1 mM EDTA (HFE) at 5 million cells/mL and incubated with indicated antibodies and cell-viability markers on ice for 30 min. After 3× washes in HFE, cells were resuspended in HFE at 5 million cells/mL and kept on ice pending analysis. Single (fixed FSC-A/FSC-W ratio) and live cells (PI- or 7AAD-negative) were gated for analysis and sorting. For flow cytometric analysis, 7AAD (BD Pharmingen; catalog no. 51-68981E) was used as the viability marker with FACSCalibur (Becton Dickinson). For sorting, propidium iodide (PI) (BD Pharmingen; catalog no. 550825) was used for selecting live cells in 13 color FACSAria (Becton Dickinson) with 488-nm blue laser at 20 PSI (Hospital for Sick Children–University Health Network Flow Cytometry Facility).

Histology and Immunofluorescence Staining. Tissue sections were deparaffinized twice with xylene for 10 min each and sequentially hydrated with 100%, 90%, 70%, and 50% ethanol in PBS. For antigen retrieval, slides were boiled in a microwave in 10 mM sodium citrate solution (pH 6.0) for ≥10 min, followed by 30 min of gradual cooling at room temperature. Sections were incubated with M.O.MMouse Ig blocking reagent for one hour (Vector M.O.M Immunodetection kit; Vector Laboratories; catalog no. 2202), followed by incubation with primary antibodies diluted in M.O.M in a humidified chamber at 4 °C overnight. Secondary antibodies (goat-anti-rabbit Alexa 488 and goat-anti-mouse Alexa 568, both 1:200 dilution) plus DAPI were added for 1 h at room temperature. The slides were mounted with DakoCytomation fluorescence medium. Primary antibodies were against mouse keratin18 (K18, 1:200 dilution; Fitzgerald; no. RDI-PR061028), keratin14 (K14, 1:200 dilution; Panomics; no. E2624), HER2 (CalBiochem; 1:200 dilution; no. OP16), Jagged1 (Cell Signaling; 1:200 dilution; no. 2620), Vimentin (Santa Cruz Biotechnology; 1:200 dilution; no. SC32322). We note that TIC frequency is reproducibly higher (twofold) after positive immunoselection with EasySep beads compared with cell sorting. However, as opposed to FACS, which allows single cell purification, immunopurification gives rise to clumps of two or more cells.

Transplantation. For picking single cells, CD24$^+$:JAG1$^-$ cells were diluted to 1 cell/10 μL, and 10 μL was seed into each well on Terasaki plates. After 30 min to allow cells for settling on the bottom of each well, the presence of a single cell/well was confirmed by microscopic examination. Single cells in 10 μL were mixed with 10 μL of matrigel (BD Bioscience #356234) on ice. Samples (total, 20 μL) were injected into no. 4 mammary glands of 3–5 wk old FVB, Rag1$^{-/-}$, SCID-Beige (Jackson and Charles River) or MMTV-Neu female mice under isoflurane anesthesia. Liquid bandage (New-Skin; no. 1310206; Prestige Brands) was applied to prevent sample leakage; wounds were closed by 9-mm autoclip (Clay Adams; no. 427631) and removed 2 wk postsurgery.

Microarray Analysis. Microarray analysis was carried out using Illumina Mouse Ref-8 v2 with 500 ng of total RNA at the Centre for Applied Genomics (HSC, Toronto). Total RNA from tumor tissue was prepared using the double TRIzol method. In short, tumor samples were minced using a razor blade, resuspended in 1 mL TRIzol and incubated on ice for 20 min. Chloroform (200 μL) was added and samples shaken at 1200 rpm for 10 min at room temperature. After centrifuging the samples at 13,000 rpm for 10 min, the upper aqueous layer was transferred to a new tube and RNA precipitated with 600 μL isopropanol. Samples were centrifuged at 16,000 × *g* for 10 min at 4 °C and supernatants removed. RNA pellets were air-dried, 5 min, and resuspended in 100 μL of RNase-free H_2O, and TRIzol purification procedure was repeated once. Microarray data were first normalized by Quantile method using BeadStudio (Illumina) with the pooled result of primary MMTV-Neu tumors as reference group to generate a list of genes with significant differential expression.

Microarray data are archived in the Gene Expression Omnibus database (accession no. GSE29616; http://www.ncbi.nlm.nih.gov/geo/query/acc.cgi?acc=GSE29616).

Generation and Analysis of HER2 Signature. To generate a list of differentially expressed genes, five independent primary mammary tumors from MMTV-Neu model (N250, N261, N283, N222, N229) were harvested and tumor cells were mechanically dissociated into single cell suspension. Cells from each tumor (with the exception of N222 and N229, which were combined in a 1:1 ratio to obtain enough cells) were FACS sorted into TIC/CD24$^+$:JAG1$^-$ and non-TIC/CD24$^-$ fractions. Total RNA purified from the eight samples using PicoPure RNA Isolation Kit (Arcturus) was subject by Affymetrix Mouse Gene 1.0 st microarray analysis at the Centre of Applied Genomics (Hospital for Sick Children). Data are archived in the NCBI GEO database (accession no. GSE29590; http://www.ncbi.nlm.nih.gov/geo/query/acc.cgi?acc=GSE29590).

Microarray data were normalized using RMA method via Partek software and log 2-transformed gene expression values were obtained. Paired *t* test statistics were performed between the TIC and $CD24^-$ fractions to identify significantly ($P < 0.05$) and differentially (>2.0-fold) expressed genes. Seventy-three genes were significantly up-regulated in the TIC fraction, and 256 genes were significantly up-regulated in the $CD24^-$ fraction. The prognostic value of each gene was assessed using GSE3143 dataset as a training set. Out of a total of 329 differentially regulated (TICs versus non-TICs) mouse genes, 284 human genes were found in the GPL8300 platform of GSE3143 dataset. The expression data were median-centered for each gene with all of the samples in the cohort. Selection of $HER2^+$ patients was based on a published method using the five genes in the HER2 amplicon (ErbB2, Stard3, Perld1, Grb7, C17orf37). A patient was considered to be $HER2^+$ if at least three of the five genes were expressed twofold above median. We tested the method with 11 published databases containing HER2 IHC results (GSE24185, GSE22358, GSE25066, GSE2603, GSE5460, GSE21653, GSE26639, GSE19697, GSE17907, GSE16446, GSE20194; Fig. S7) and determined that at twofold cutoff, 80.7% of the amplicon-selected patients were also $HER2^+$ by IHC and 69.5% of total IHC $HER2^+$ samples were included.

Using all 284 genes differentially regulated in TICs, the $HER2^+$ patients were divided into two groups using the formula:

$$\text{Score for Signature Match (SSM)} = \sum(I_n X_n/|X_n|)/\sum(|I_n|)$$

Where I is the gene index; 1 for up-regulated genes in TICs and −1 for down-regulated genes. X is the log 2 transformed and median-centered gene expression value of the patient; n indicates signature gene number. SSM ≥0 was considered to be a match to the signature. Using these criteria, the 284 differentially regulated TIC genes identify a group of $HER2^+$ patients with poor prognosis (HR, 2.54; $P = 0.072$; Fig. S8*A*) in the GSE3143 dataset. To further improve the signature, $HER2^+$ patients were divided into poor (OS, 1) and good (OS, 0). Ward agglomerative clustering divided the poor group of $HER2^+$ patients into two subgroups: Cluster1 with the average survival of 34 mo; and Cluster2 with the average survival of 48 mo. We used a scoring algorithm that calculates the association of the expression of the gene to a particular patient group:

$$\text{Gene Association(GA)} = \left(\sum X_i/|X_i|\right)\Big/ n$$

Where X is the expression of the gene and n is the number of patients in the given group. For up-regulated genes in TICs, a criterion of GA score > 0.5 in cluster1 or cluster2 was used, and 10 genes were found to be qualified. For down-regulated genes, we set the criterion to be GA score <−0.5 in cluster1 or cluster2 and also a positive association of GA > 0.3 with good-prognosis group. 48 down-regulated genes met this criterion. The combined 40 genes were used to analyze patient prognosis and an improved prediction was achieved (HR, 3.53; $P = 0.00742$; Fig. S8*A*). Finally, we performed progressive elimination analysis by adjusting the cutoff value for the GA score with good-prognosis group of patients. For up-regulated genes, a cutoff of GA < 0.2 was determined for both cluster1 and cluster2, and eight genes (Aurkb, Cldn8, Npy, Atp7b, Chaf1b, Scrn1, Ccna2, Ccnb1) were selected. For down-regulated genes, a cutoff was set at GA > 0.4 for cluster1 and GA > 0.3 for cluster2; nine genes (Nrp1, Cd74, C1qb, Cd72, Vcam1, Itgb2, Cd180, Ccr2, St8sia4) passed the criteria. The resulting 17-gene signature, HTICS, gave the best prediction on patient outcome in GSE3143 dataset (HR, 5.24; $P = 0.000491$; Fig. 4*A*).

To validate the signature, we used HTICS to analyze six datasets with overall survival data (GSE1456, GSE3494, GSE7390, GSE16446, GSE18229, GSE20685), of which four also had ERα status (GSE3494, GSE7390, GSE16446, GSE18229). In addition, the status of p53 mutation was provided by GSE3494. In addition, six datasets with MFS data (GSE2034, GSE2603, GSE 5327, GSE6532, GSE11121, GSE25066) were used; four of which provided ERα status (GSE2034, GSE2603, GSE6532, GSE25066). Finally, two datasets with DFS data were analyzed (GSE4922, GSE12093). A total of 14 datasets were included across 10 different Affymetrix and Agilent platforms (GPL8300, GPL96, GPL570, GPL885, GPL887, GPL1390, GPL1708, GPL5325, GPL6607, GPL7504).

Two datasets with pathological complete response (pCR) information were analyzed: GSE22358 and the MD Anderson cohorts. For pCR analysis, only samples with complete responses (pCR) were considered to be success and all other responses (partial, minor, near-complete) were regarded as failure. SSM for HTICS was calculated for each sample and number of patients with success/failure in $HTICS^-/HTICS^+$ groups was assessed by χ^2 test to determine significance. For postsurgery analysis, such as % metastasis and overall survival/MFS Kaplan–Meier curves, tow samples (one $HER2^+$:$ER\alpha^+$, one $HER2^+$:$ER\alpha^-$) were removed from the MD Anderson cohort because of a different adjuvant chemotherapy regimens. For percentage metastasis analysis, $HER2^+$:$ER\alpha^-$ samples from published cohorts were combined as $Trastuzumab^-$ group and used to compare with the Trastuzumab-treated ($trastuzumab^+$) patients from MD Anderson. Statistical significance was calculated by χ^2 test.

Each dataset was analyzed independently by obtaining RMA normalized expression value of the individual cohort for log 2 transformation and median-centering. $HER2^+$ patients were then selected by amplicon method for signature analysis with SSM algorithm. The comparison with additional signatures was done with SSM algorithm for all signatures to ensure equal comparison. Kaplan–Meier and survival analysis were performed with PAST program (P.D. Ryan and Ø. Hammer, University of Oslo, Norway), and *P* values was calculated by Wilcoxon method. HRs were obtained using the COX proportional hazards survival regression method. Heat maps and dendrograms were generated by JAVA tree-view.

Pathway Analysis. The data were analyzed by GSEA (4) using paired *t* test comparing gene expression values in the TIC and $CD24^-$ fractions, and parameters set to 2,000 gene-set permutations, gene-sets size between 15 and 500. An enrichment map [version 1.1 of Enrichment Map software (5)] was generated using enriched gene sets with a nominal *P* value of <0.005, FDR of <1%, and the overlap coefficient set to 0.5. The databases included in the GSEA analyses were the Gene Ontology (GO), Kyoto Encyclopedia of Genes and Genomes (KEGG), Protein Families Database (PFAM), BioCarta, and National Cancer Institute (NCI) databases. GO, PFAM and KEGG annotations were downloaded from Bioconductor (org.Mm.eg.db version 2.4.6; GO.db version 2.4.5; KEGG.db version 2.4.5). NCI annotations were downloaded from the NCI Web site (http://pid.nci.nih.gov), and BioCarta annotations were downloaded from WhichGenes. In Fig. 3, node size corresponds to the number of genes in the gene set, which are connected by edges when they have genes in common, with line width corresponding to the number of shared genes.

Additional Statistical Analysis. Paired samples were analyzed by Student *t* test. Significance of comparing multiple samples was calculated using ANOVA and the Bonferroni test for post hoc analysis. Differences between values were considered statistically significant at $P < 0.05$. TIC frequency and 95% confidence intervals were calculated using L-Calc (StemCell Technologies).

1. Guy CT, et al. (1992) Expression of the neu protooncogene in the mammary epithelium of transgenic mice induces metastatic disease. *Proc Natl Acad Sci USA* 89:10578–10582.
2. Liu JC, Deng T, Lehal RS, Kim J, Zacksenhaus E (2007) Identification of tumorsphere- and tumor-initiating cells in HER2/Neu-induced mammary tumors. *Cancer Res* 67:8671–8681.
3. Jiang Z, et al. (2010) Rb deletion in mouse mammary progenitors induces luminal-B or basal-like/EMT tumor subtypes depending on p53 status. *J Clin Invest* 120:3296–3309.
4. Subramanian A, et al. (2005) Gene set enrichment analysis: A knowledge-based approach for interpreting genome-wide expression profiles. *Proc Natl Acad Sci USA* 102:15545–15550.
5. Merico D, Isserlin R, Stueker O, Emili A, Bader GD (2010) Enrichment map: A network-based method for gene-set enrichment visualization and interpretation. *PLoS ONE* 5: e13984.

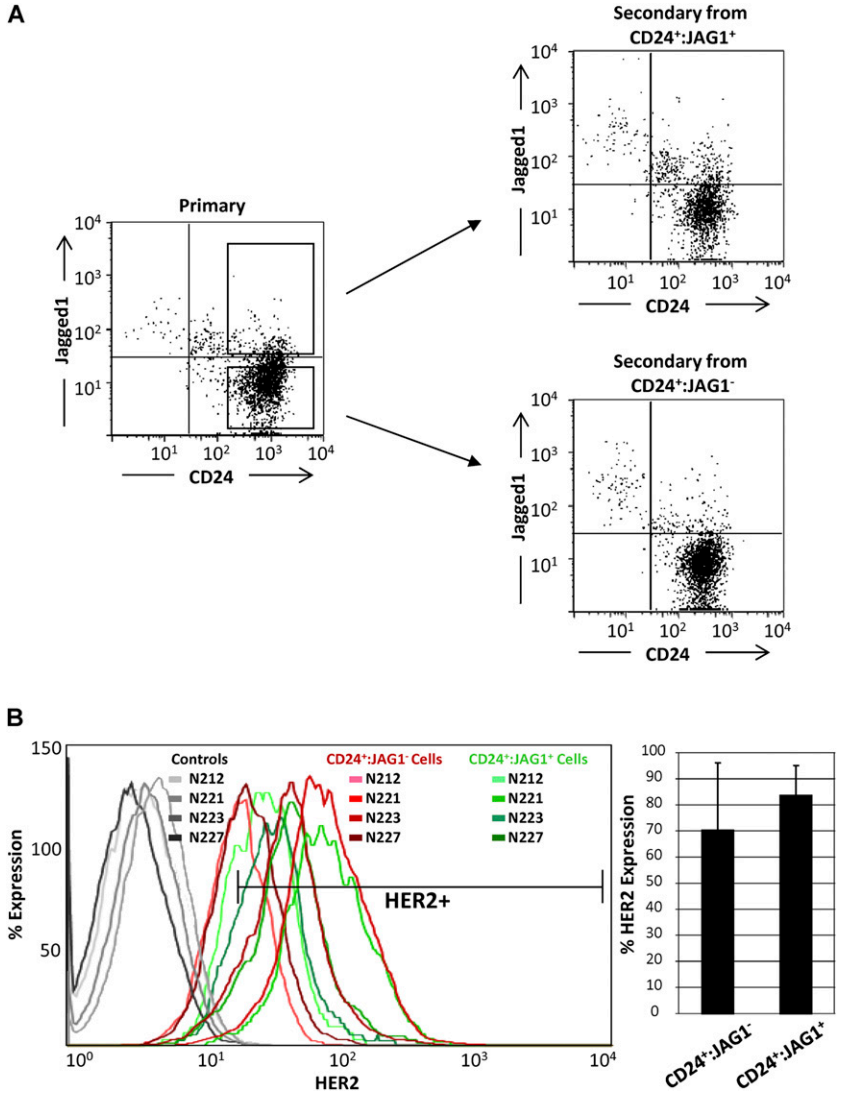

Fig. S1. (*A*) TICs in CD24$^+$:JAG1$^+$ and CD24$^+$:JAG1$^-$ fractions regenerate the cellular complexity of Neu mammary tumors. (*A*, *Left*) Flow cytometric profile of a primary Neu tumor and gated CD24$^+$:JAG1$^+$ and CD24$^+$:JAG1$^-$cells used for transplantation. (*A*, *Right*) Flow cytometric profiles of secondary tumors derived from transplantation of 500 CD24$^+$:JAG1$^+$ (*Upper*) or CD24$^+$:JAG1$^-$ (*Lower*) cells, demonstrating that both fractions regenerated the cellular complexity seen in primary Neu tumors. (*B*) Similar expression of HER2 in CD24$^+$:JAG1$^-$ and CD24$^+$:JAG1$^+$ fractions. (*B*, *Left*) Levels of HER2/NEU expression in CD24$^+$:JAG1$^-$ and CD24$^+$:JAG1$^+$ populations estimated by flow cytometric analysis of four independent tumors (N212, N221, N223, and N227). (*B*, *Right*) average expression of HER2/NEU in the CD24$^+$:JAG1$^-$ and CD24$^+$:JAG1$^+$ fractions based on the flow cytometric analysis (n = 4).

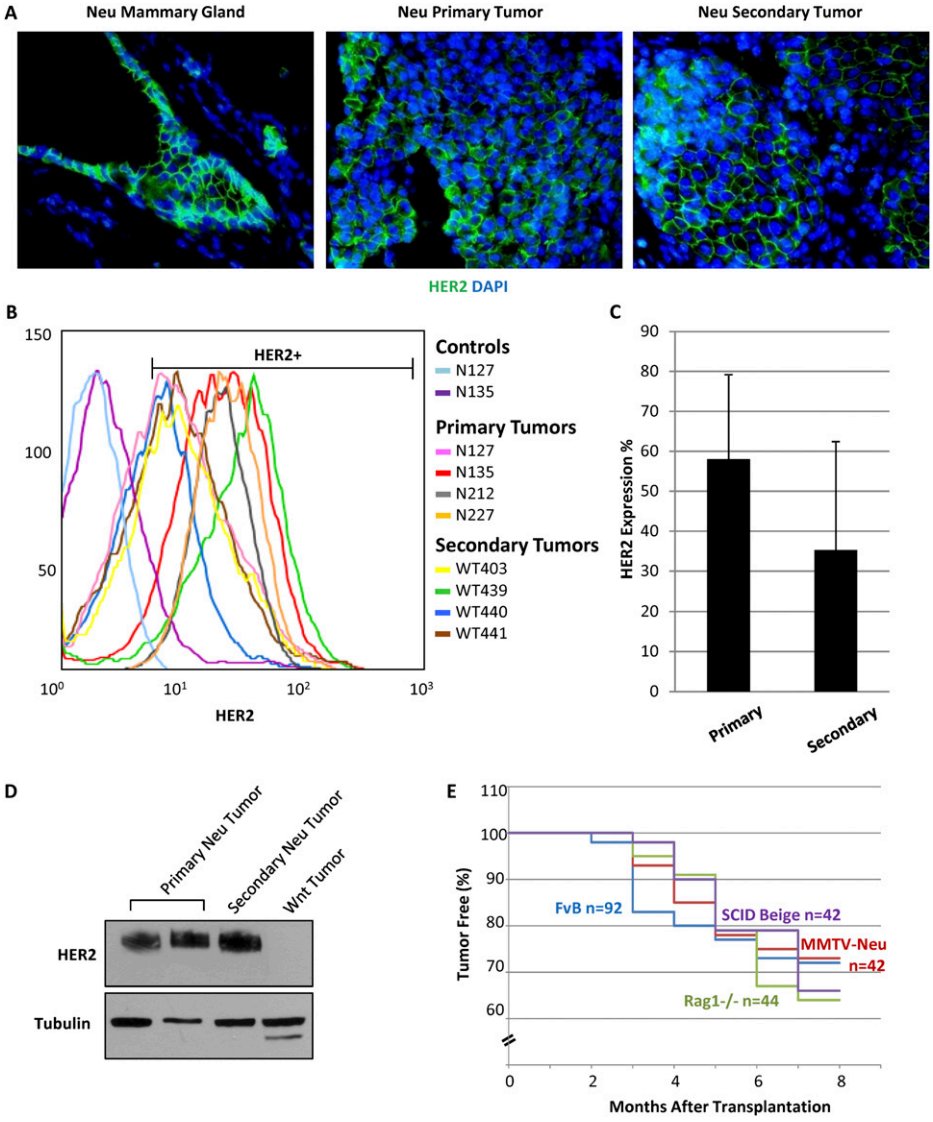

Fig. S2. Expression of HER2/NEU in primary and secondary MMTV-Neu tumors, and transplantation efficiency in isogenic versus immunocompromised mice. (*A*) Representative immunofluorescent staining for HER2/NEU (green) in MMTV-Neu mammary gland, primary, and secondary tumors. DAPI was used to stain nuclei (blue). (*B*) HER2/NEU expression quantified by flow cytometric, comparing four primary tumors (N127, N135, N212, and N227) to four secondary tumors induced in FvB host (WT403, WT439, WT440, and WT441). (*C*) Percentage of HER2/NEU expression in the primary and secondary tumors shown in *B*, demonstrating non-statistically significant reduction in protein expression in secondary tumors. (*D*) Western blot analysis for HER2/NEU in primary and secondary tumors. Protein lysate from a MMTV-Wnt1 tumor was used as negative control. Tubulin served as a loading control. (*E*) Kaplan–Meier tumor-free curve for sorted MMTV-Neu $CD24^{+}$ tumor cells transplanted into the mammary glands of 3–5-wk-old syngeneic FvB mice (n = 92 injection), MMTV-Neu mice (n = 42), immunodeficient $Rag1^{-/-}$ (n = 44), and SCID Beige mice (n = 42), demonstrating that transplantation efficiency of MMTV-Neu tumor cells is similar in immunocompetent and immunocompromised mice.

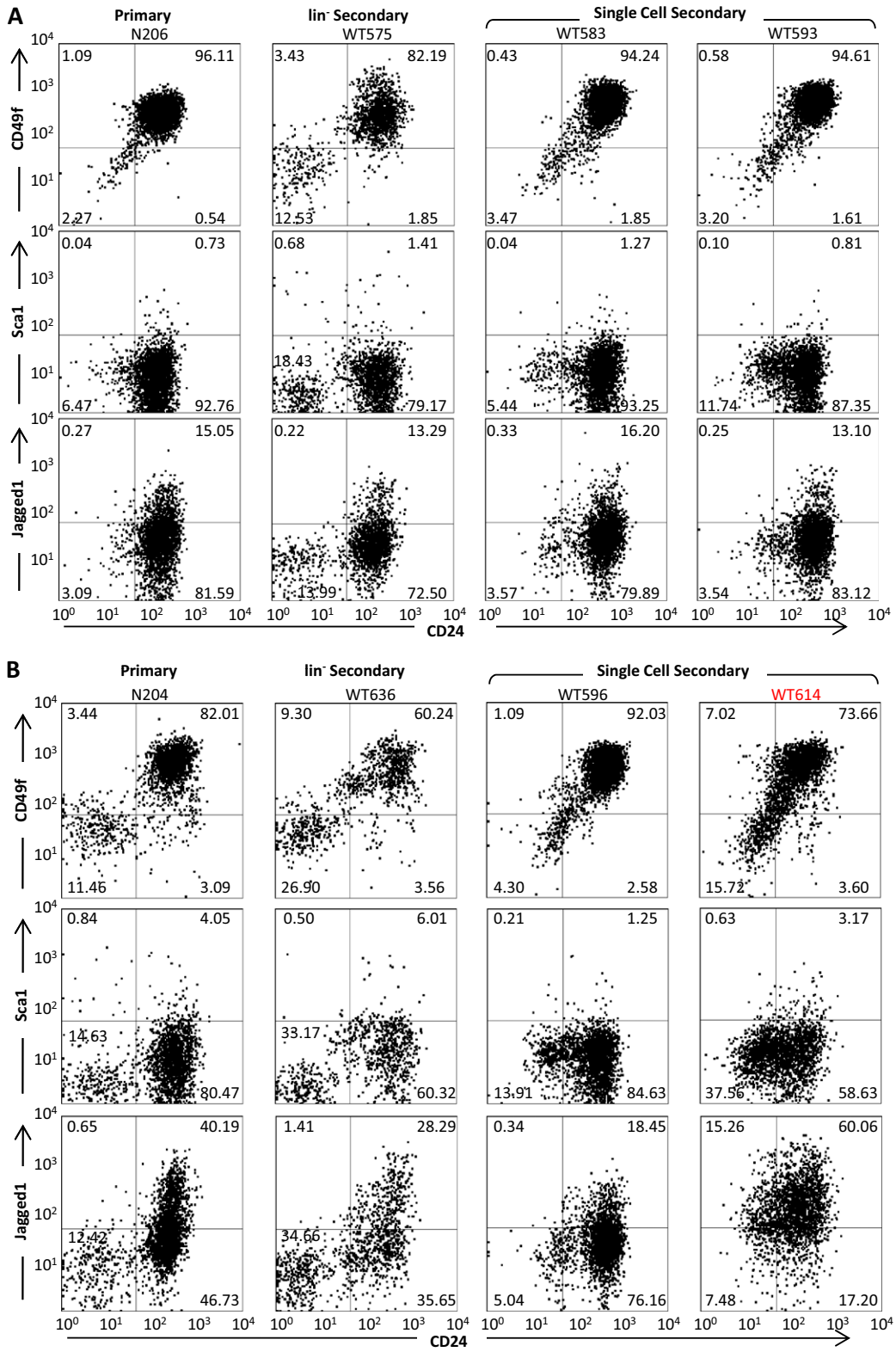

Fig. S3. (Continued)

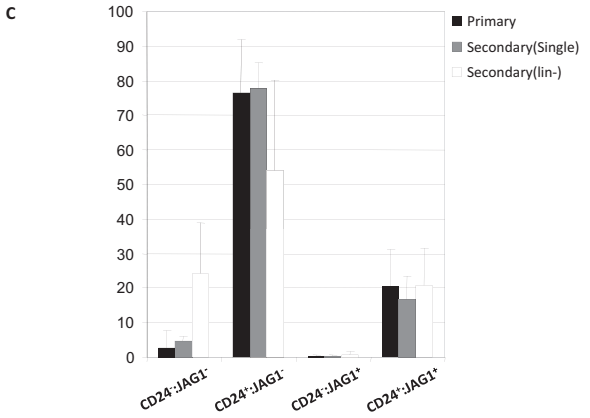

Tumor	$CD24^-:JAG1^-$	$CD24^+:JAG1^-$	$CD24^-:JAG1^+$	$CD24^+:JAG1^+$
Primary Tumors (n=6)	2.6 ± 4.9	76.5 ± 15.3	0.4 ± 0.2	20.5 ± 10.8
Secondary Single Cell Tumors (n=7)	4.8 ± 1.1	78.0 ± 7.1	0.4 ± 0.2	16.8 ± 6.7
Secondary lin^- Tumors (n=2)	24.3 ± 14.6	54.1 ± 26.1	0.8 ± 0.8	20.8 ± 10.6

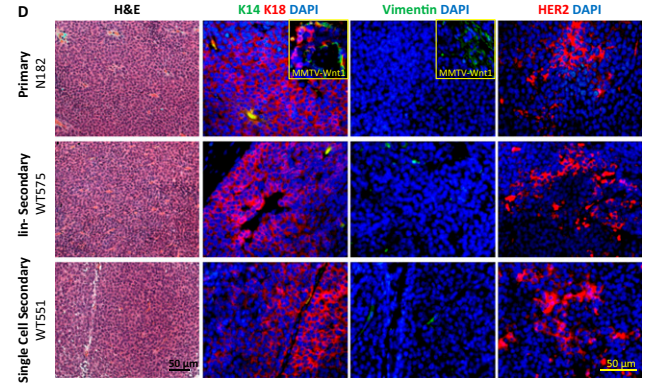

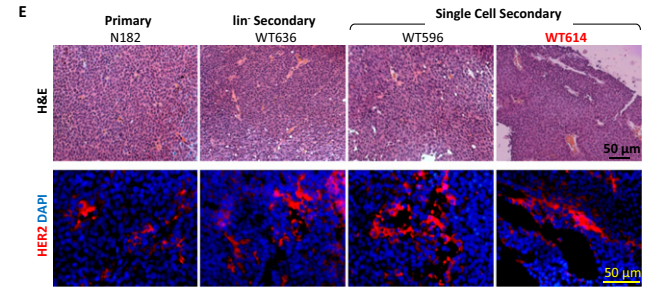

Fig. S3. (Continued)

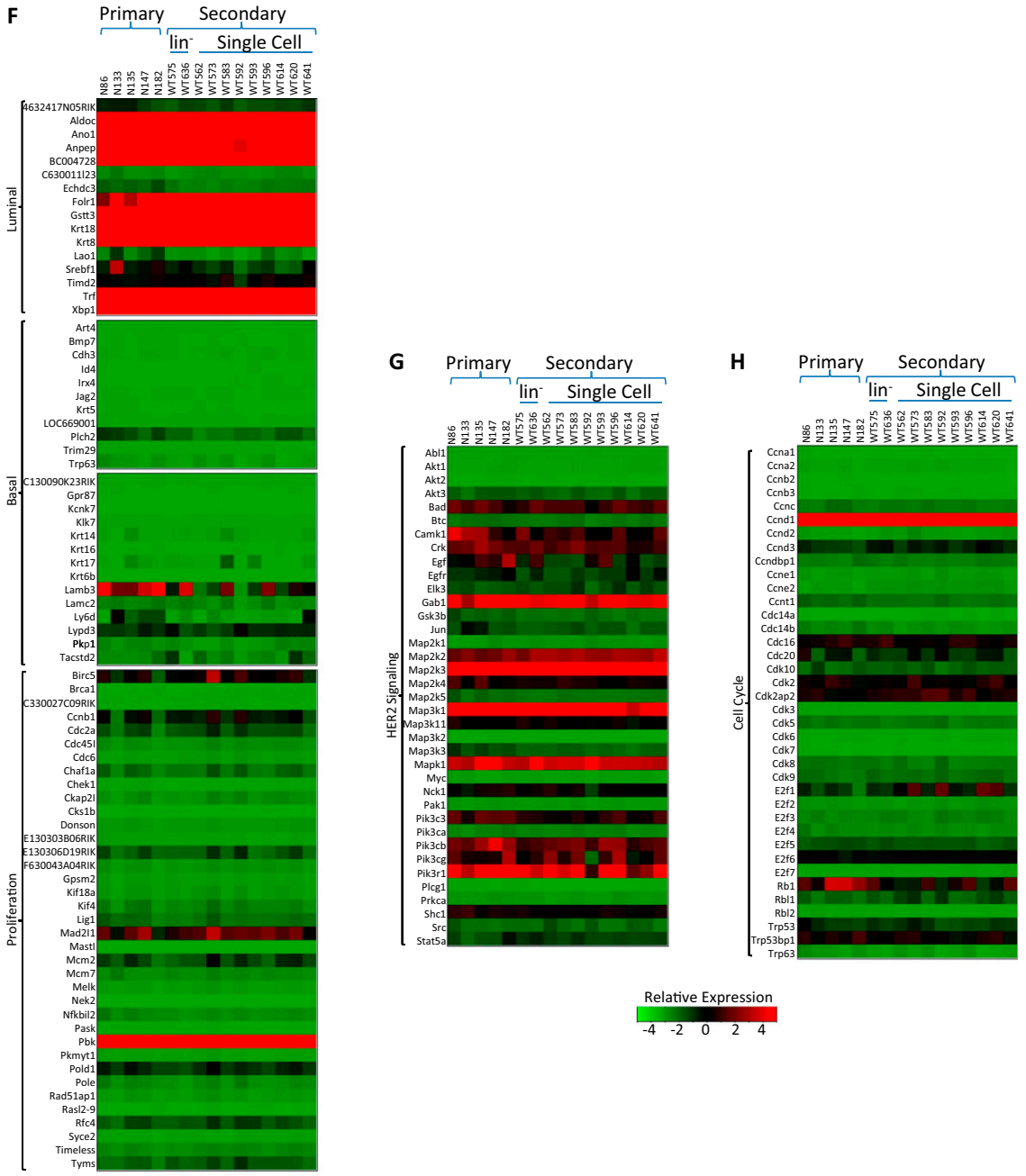

Fig. S3. (Continued)

I

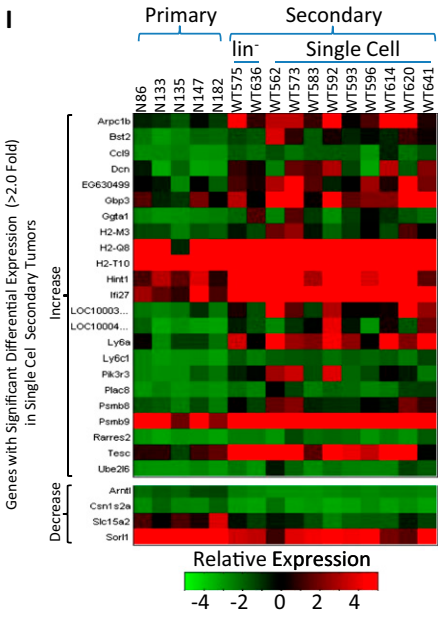

J

List of Genes with Significant Decrease of Expression (≤0.5X) in Single Cell Secondary Tumors

Gene	Fold	Description
Lamb3	0.4	Mus musculus laminin, beta 3 (Lamb3), mRNA.
Slc15a2	0.4	Mus musculus solute carrier family 15 (H+/peptide transporter), member 2 (Slc15a2), mRNA.
Arntl	0.5	Mus musculus aryl hydrocarbon receptor nuclear translocator-like (Arntl), mRNA.
Sorl1	0.5	Mus musculus sortilin-related receptor, LDLR class A repeats-containing (Sorl1), mRNA.

K

List of Genes with Significant Increase of Expression (≥2X) in Single Cell Secondary Tumors

Gene	Fold	Description
Ifi27	5.3	Mus musculus interferon, alpha-inducible protein 27 (Ifi27), mRNA.
LOC100038882	3.7	PREDICTED: Mus musculus hypothetical protein LOC100038882 (LOC100038882), mRNA.
Ly6a	3.3	Mus musculus lymphocyte antigen 6 complex, locus A (Ly6a), mRNA.
Bst2	3.3	Mus musculus bone marrow stromal cell antigen 2 (Bst2), mRNA.
Arpc1b	2.6	Mus musculus actin related protein 2/3 complex, subunit 1B (Arpc1b), mRNA.
Psmb8	2.4	Mus musculus proteasome (prosome, macropain) subunit, beta type 8 (large multifunctional peptidase 7) (Psmb8), mRNA.
Plac8	2.3	Mus musculus placenta-specific 8 (Plac8), mRNA.
Psmb9	2.3	Mus musculus proteasome (prosome, macropain) subunit, beta type 9 (large multifunctional peptidase 2) (Psmb9), mRNA.
Ly6c1	2.3	Mus musculus lymphocyte antigen 6 complex, locus C1 (Ly6c1), mRNA.
Hint1	2.2	Mus musculus histidine triad nucleotide binding protein 1 (Hint1), mRNA.
Rarres2	2.2	Mus musculus retinoic acid receptor responder (tazarotene induced) 2 (Rarres2), mRNA.
Ube2l6	2.2	Mus musculus ubiquitin-conjugating enzyme E2L 6 (Ube2l6), mRNA.
H2-T10	2.1	Mus musculus histocompatibility 2, T region locus 10 (H2-T10), mRNA.
Ccl9	2.0	Mus musculus chemokine (C-C motif) ligand 9 (Ccl9), mRNA.
H2-Q8	2.0	Mus musculus histocompatibility 2, Q region locus 8 (H2-Q8), mRNA.
H2-M3	2.0	Mus musculus histocompatibility 2, M region locus 3 (H2-M3), mRNA.

Fig. S3. Single-cell-derived tumors are indistinguishable from primary MMTV-Neu tumors. (*A* and *B*) Representative flow cytometric profiles for CD24 plus CD49f, Sca1, or Jagged1 of representative primary, lin$^-$-derived, and single-cell-derived (CD24$^+$:JAG1$^-$) Neu tumors. The outlier WT614 exhibits high level of CD24-JAG1 double positive cell population but similar profiles for CD24-Sca1 and CD24-CD49f. (*C*) Distribution of cells according to CD24-JAG1 expression is similar in single cell-derived and primary tumors. Graphic presentation (*Upper*) and numerical data (*Lower*) for CD24-JAG1 expression in primary versus lin$^-$-derived, or single-cell-derived (CD24$^+$:JAG1$^-$) secondary tumors, showing similar distribution of CD24$^+$:JAG1$^-$ and CD24$^+$:JAG1$^+$ cells across multiple samples. (*D* and *E*) Histology (hematoxylin/eosin staining) and immunofluorescent analysis of representative primary, lin$^-$-derived, and single-cell-derived tumors for keratin14 (K14, green), keratin18 (K18, red), vimentin (green), and HER2/NEU (red). DAPI was used to label nuclei (blue). Note similar histology and marker expression in the various tumors including the WT614 outlier. (*F–H*) Representative microarray expression profiles of primary, lin$^-$-derived, and single-cell-derived Neu tumors showing that single-cell-derived tumors exhibit similar gene profiles and cluster together. Heat maps for selected genes representing the luminal gene cluster and basal and proliferation markers (*F*); the HER2 signaling pathway (*G*); cell cycle markers (H). (*I–K*) Differentially expressed genes identified by microarray analysis of single-cell-derived tumors versus primary and lin$^-$-derived MMTV-Neu tumors. (*I*) A heat map for 20 genes (of the 25,600 genes on the Illumina chip) with significant difference in expression (≥2) in single-cell-derived tumors versus primary or lin$^-$-derived tumors. (*J*) Genes with significant decrease of expression (≤0.5×) in single cell-derived tumors. (*K*) Genes with significant increase of expression (≥2.0×) in single cell-derived tumors. Note abundance of IFN-associated factors: Ifl27, Ly6a, Ly6c, Ccl9, H2-T10, H2-Q8, H2-M3.

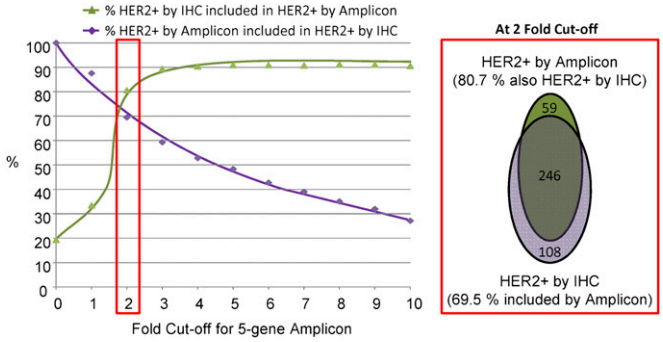

Fig. S4. Comparison of HER2$^+$ patient selection by IHC versus the five-gene HER2 amplicon. Samples from 11 published cohorts were combined and the percentage overlap between the two methods of choosing HER2$^+$ patients was calculated at increasing cutoff values of the five HER2 gene amplicon (ErbB2, Stard3, Perld1, Grb7, C17orf37). (*Left*) Green line, percentage of HER2$^+$ patients selected by the amplicon that is also HER2$^+$ based on IHC. Blue line, percentage of total HER2$^+$ patients selected by IHC included in the selected samples. With higher cutoff, fewer HER2$^+$ samples are included in the study. (*Right*) Optimal percentage is achieved at twofold cutoff: 80.7% of selected samples are both HER2$^+$ by amplicon and by IHC, whereas 69.5% of total HER2$^+$ by IHC samples are included.

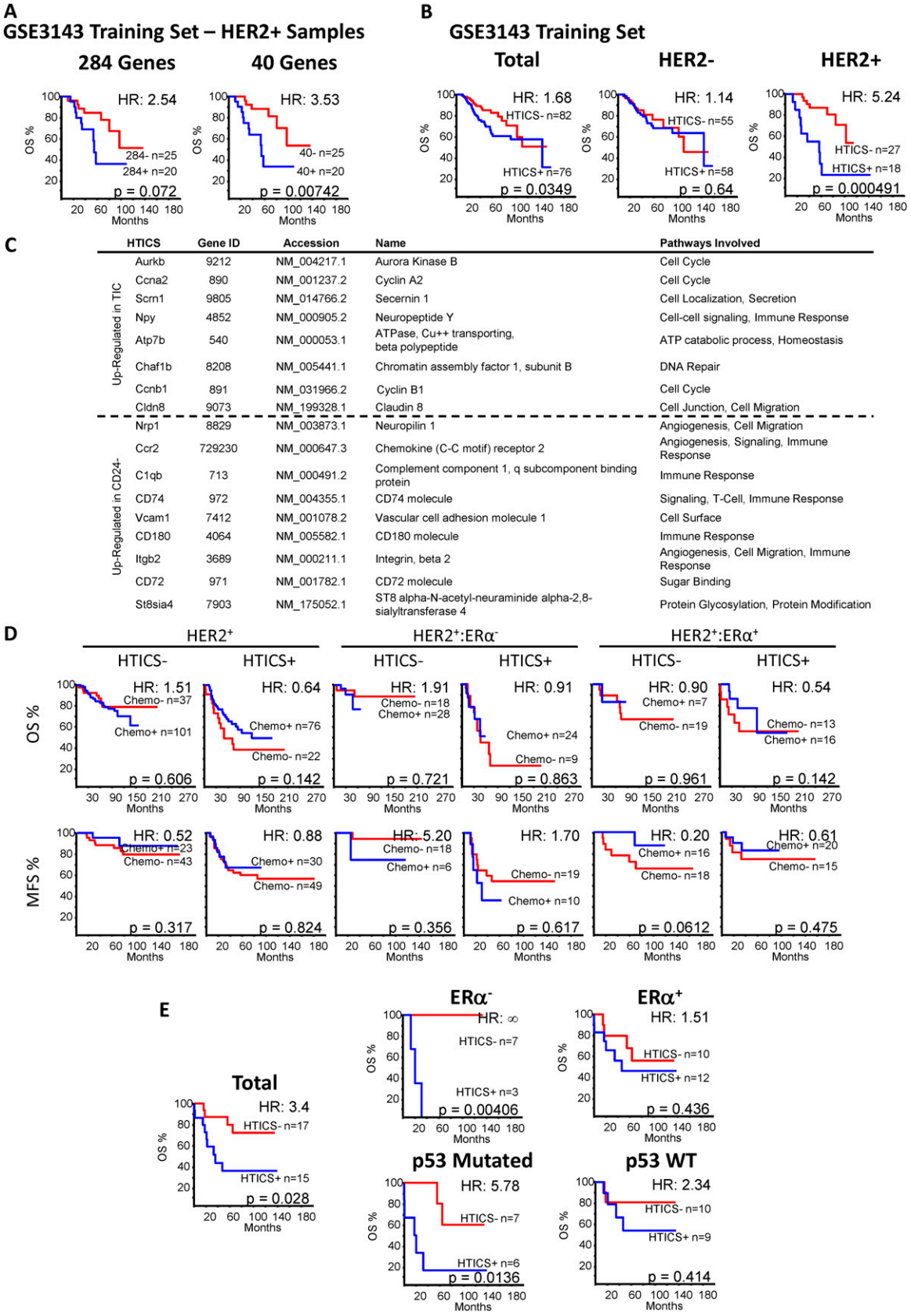

Fig. S5. Generation and predictive power of HTICS. (*A*) Stepwise generation of HTICS and specificity for HER2$^+$ patients. Kaplan–Meier OS curves for the 284 and 40 gene signatures derived from differentially expressed genes in TICs versus non-TICs in the GSE3143 training cohort. HTICS was derived from the 40 gene signature (Fig. 4*A*). (*B*) HTICS predicts outcome for HER2$^+$ patients (HR, 5.24; $P = 0.00049$) but not for all BC or HER2$^-$ patients. (*C*) List of HTICS genes, names,

Legend continued on following page

and functions. (*D*) Retrospective analysis showing that HER2$^+$:ERα$^-$ BC patients exhibit poor response to conventional chemotherapy. Kaplan–Meier curves of HER2$^+$, HER2$^+$:ERα$^-$, and HER2$^+$:ERα$^+$ BC patients subdivided by HTICS$^{+/-}$ status was used to determine the efficacy of systemic chemotherapy with all six OS and six MFS test cohorts. A tendency of HER2$^+$ and HER2$^+$:ERα$^+$, but not HER2$^+$:ERα$^-$ patients, to benefit from chemotherapy was observed for both the OS and MFS analysis. (*E*) p53 status affects HTICS prognostic power. OS for HER2$^+$ tumors in the GSE3494 set, which provides p53 and ERα status, for all patients (*Left*), or patients divided on the basis of ERα expression (*Upper*) or p53 mutant versus wild-type (*Lower*).

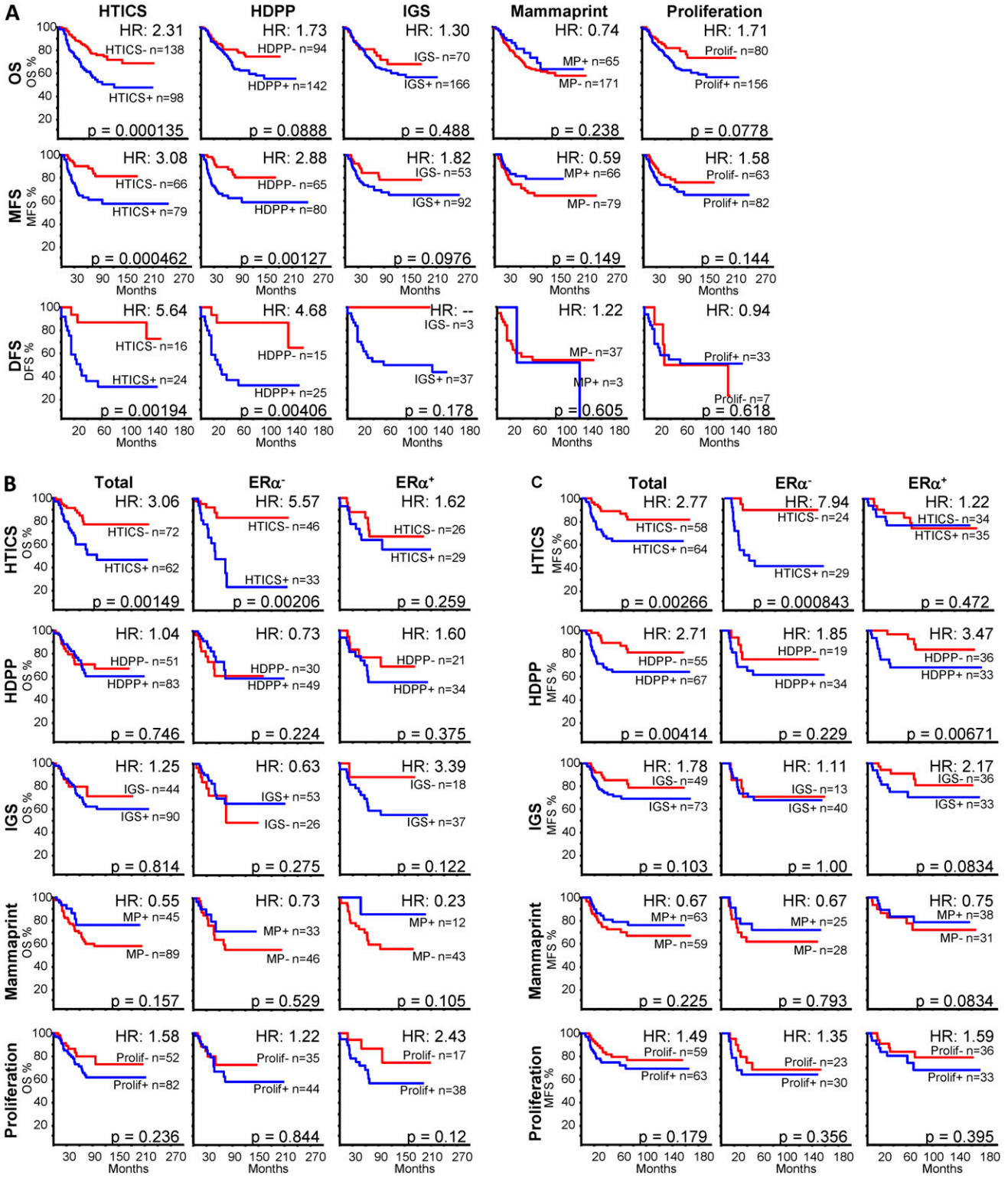

Fig. S6. Predictive powers of HTICS versus HDPP, IGS, MammaPrint, and proliferation signatures. (*A*) OS, MFS, and DFS Kaplan–Meier curves of HER2$^+$ patients based on HTICS, HDPP, IGS, MammaPrint, and proliferation signature. (*B* and *C*) Kaplan–Meier OS (*B*) and MFS (*C*) curves of HER2$^+$, HER2$^+$:ERα$^-$, and HER2$^+$:ERα$^+$ patients based on HTICS, HDPP, IGS, MammaPrint, and proliferation signature.

Bivariate Analysis of HTICS with each of the following variables for HER2⁺ patients (from 3 - 6 Test OS Cohorts)

Variables	Overall Survival n+	n-	p Value	Hazard Ratio (95% CI)
ERα (+/-)	55	79	0.57	0.83 (0.43 – 1.59)
+HTICS	62	72	0.0013	3.14 (1.56 – 6.32)
Chemo (+/-)	177	59	0.798	0.94 (0.56 – 1.56)
+HTICS	98	138	0.0004	2.32 (1.46 – 3.70)
Grade ≥ 3	100	47	0.728	1.12 (0.60 – 2.07)
+HTICS	66	81	0.0056	2.36 (1.29 – 4.33)
Age ≥ 50	88	100	0.676	1.11 (0.68 – 1.82)
+HTICS	78	110	0.0002	2.62 (1.59 – 4.33)
Node (+/-)	62	69	0.0001	4.21 (2.01 – 8.85)
+HTICS	61	70	0.0063	2.74 (1.33 – 5.65)
Size ≥ 2 cm	75	27	0.462	1.35 (0.61 – 3.01)
+HTICS	46	56	0.0054	2.75 (1.35 – 5.60)
Univariate Analysis of HTICS on Subgroups with Significantly Increased HR				
	Node+			
HTICS	35	27	0.0238	3.12 (1.16 – 8.35)

Bivariate Analysis of HTICS with each of the following variables for HER2⁺:ERα⁻ patients (from 3 - 6 Test OS Cohorts)

Variables	Overall Survival n+	n-	p Value	Hazard Ratio (95% CI)
Chemo (+/-)	52	27	0.886	1.08 (0.40 – 2.88)
+HTICS	33	46	0.0012	5.52 (1.97 – 15.51)
Grade ≥ 3	63	15	0.268	0.59 (0.23 – 1.50)
+HTICS	33	45	0.0016	5.26 (1.88 – 14.71)
Age ≥ 50	26	22	0.57	1.31 (0.51 – 3.35)
+HTICS	18	30	0.0008	5.92 (2.08 – 16.81)
Node (+/-)	40	37	0.0332	3.28 (1.10 – 9.79)
+HTICS	33	44	0.0027	5.69 (1.83 – 17.74)
Size ≥ 2 cm	36	11	0.889	1.08 (0.35 – 3.40)
+HTICS	17	30	0.0014	5.66 (1.96 -16.34)
Univariate Analysis of HTICS on Subgroups with Significantly Increased HR				
	Node+			
HTICS	21	19	0.0321	5.20 (1.15 – 23.5)

Multivariate Analysis of HTICS with all variables for HER2⁺:ERα⁻ patients (3 Test OS Cohorts)

Variables	Overall Survival n+	n-	p Value	Hazard Ratio (95% CI)
HTICS	17	27	0.0051	6.27 (1.73 -22.67)
Chemo (+/-)	18	26	0.8	1.20 (0.30 – 4.80)
Grade ≥ 3	32	12	0.4213	1.66 (0.48 – 5.66)
Age ≥ 50	24	20	0.2803	1.92 (0.59 -6.27)
Node (+/-)	20	24	0.0147	8.29 (1.52 – 45.39)
Size ≥ 2 cm	34	10	0.5294	0.60 (0.12 – 2.95)

Fig. S7. HTICS predicts OS independently of other predictors including Node status. The status of ER ($^{+/-}$) administration of systemic chemotherapy (excluding trastuzumab) (chemo$^{+/-}$; Dataset S1A), grade (≥3), age (≥50 y), lymph node ($^{+/-}$), and size (≥2 cm) were taken into consideration with HTICS in bi- and multivariate analysis using Cox proportional hazard model. Three OS test cohorts (GSE3494, GSE7390, GSE18229) had information on all variables and were used for multivariate analysis. In addition, the status of ERα was also available with GSE16446; administration of systemic chemotherapy included in GSE1456, GSE16446, and GSE20685; grade included in GSE1456 and GSE16446; age included in GSE20685; and node status also in GSE16446. The bivariate analysis for HER2^{+} and HER2^{+}:ERα^{-} patients was performed with all available data from the six cohorts. Additional univariate analysis was performed on the node-positive subgroup showing that HTICS can further subdivide these patients into high- and low-risk groups with HR of 5.2. The multivariate analysis demonstrates that HTICS predicts clinical outcome independently of all other predictors and can be combined with node status to increase HR.

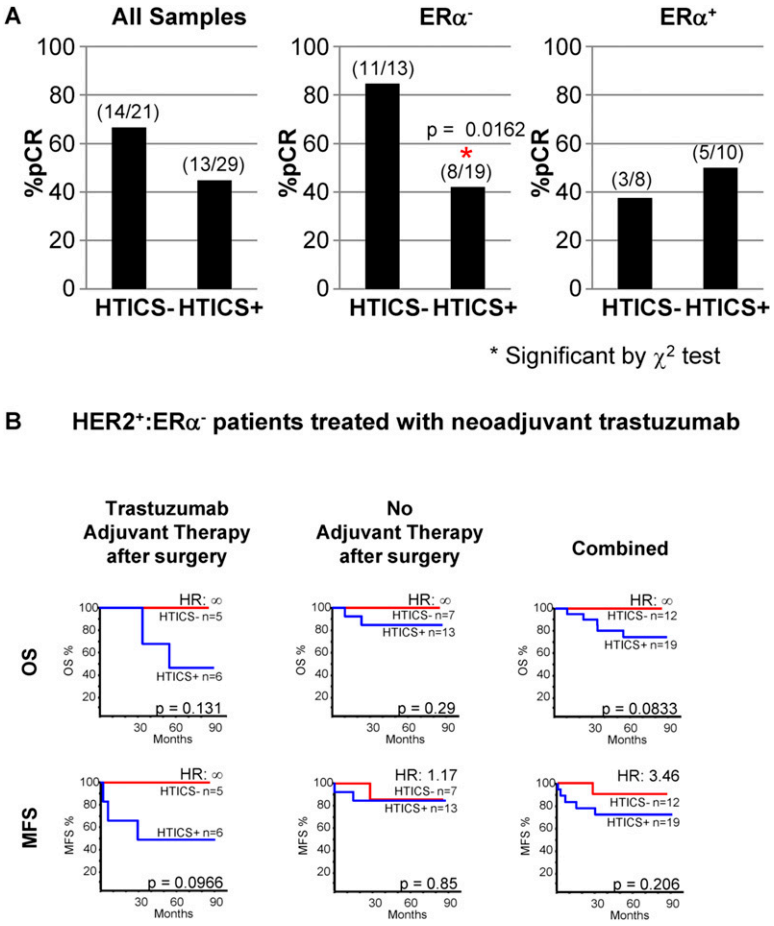

Fig. S8. Analysis of MD Anderson dataset for HER2$^+$ patients treated with neoadjuvant chemotherapy plus trastuzumab. (*A*) Percentage of pCR determined at the time of surgery. Patients were subdivided into two groups according to ERα status (determined by IHC). For ERα$^-$ patients, the HTICS$^+$ group has significant lower percentage of pCR than the HTICS$^-$ group ($P = 0.0162$, χ^2 test). Fig. 6*A* shows data on pCR after combining this MD Anderson dataset with a publicly available cohort (GSE22358; see main text). (*B*) OS and MFS analysis for HER2$^+$:ERα$^-$ patients 90 mo postsurgery. Patients were grouped according to the continuation (*Left*) or not (*Center*) of trastuzumab treatment after surgery. In both cases, no death occurred in the HTICS$^-$ group compared with five deaths in the HTICS$^+$ group ($P = 0.0833$) for the combined data. Only one patient in the HTICS$^-$ group had metastasis versus five patients with metastases in the HTICS$^+$ set ($P = 0.206$).

Other Supporting Information Files

Dataset S1 (XLSX)